NUMERICAL STUDY OF THE AIRFLOW AROUND THE AIRFOIL SELIG 1223

Daniel B.V.F. Silva and Mila R. Avelino
Departamento de Engenharia Mecânica
Universidade do Estado do Rio de Janeiro – UERJ
20550-013 - Rio de Janeiro - RJ
E-mail: mila@uerj.br

Marcelo J.S. De-Lemos
Departamento de Energia – IEME
Instituto Tecnológico de Aeronáutica – ITA
12228-900 - São José dos Campos – S.P. - Brazil
Tel: +55-12-3947.5860, FAX: +55-12-3947.5842
E-mail: delemos@mec.ita.br

Abstract. *In this work, numerical simulations are performed for the airflow through the SELIG 1223 airfoil. The numerical simulation is performed using two computer programs, namely the FLUENT code, a CFD finite-volume based software, and XFOIL, an interactive boundary-layer code. Results are presented in terms of lift and drag coefficients and pressure distributions for the chord based Reynolds number of $2x10^5$. They are calculated in FLUENT using different turbulence models, namely Spalart-Allmaras (one-equation) and Realizable k-ε (two-equation) model. For the near-wall region treatment, the low Reynolds approximation is employed. Results obtained with XFOIL, using free and forced transition, are also shown. The numerical results are compared to the experimental work of Selig et al.*

Keywords: *Numerical solution, External flow, Airfoil.*

1. INTRODUCTION

The prediction of aerodynamic characteristics of an airfoil is still a challenging task, in spite of recent developments in Computational Fluid Dynamics. There are two principal methods of obtaining the desired results (Cebeci et al, 1998) – one is the solution of the Navier-Stokes equations using structured or unstructured grids and the other is based on an interactive viscous-inviscid boundary-layer theory.

The S1223 airfoil was designed by Michael Selig for the SAE R/C small airplane competition for weight lifting. This heavy-lift airfoil was designed to provide 30% more lift than the Wortmann FX 63-137 airfoil, which to date has been one of the favorites for the competition. These airfoils are not expected to perform well much below a Reynolds number of $2x10^5$, that is the typical design Reynolds number for the competition.

2. NUMERICAL ANALYSIS USING XFOIL

2.1. Introduction to XFOIL

XFOIL is an iterative boundary layer code written by Drela (1987) for design and analysis of airfoils, which can handle both inviscid and coupled viscous-inviscid boundary layer flows. XFOIL uses a two-equation boundary layer integral formulation based on dissipation closure for both laminar and turbulent flow. It includes in the laminar formulation a transition prediction based on the spatial amplification theory. A linear model is employed to predict transition, which accounts for the growth of the amplitude n of the most amplified Tollmien-Schlichting wave (Schlichting, 1979). In the turbulent formulation it also includes a lag equation to account for lags in the response of the turbulent stresses to changing flow conditions. The inviscid freestream is computed using a linear-vorticity panel method. The boundary layer and transition equations are solved simultaneously with the inviscid flow field by a global Newton method. The boundary layers and wake are described with a two-equation lagged dissipation integral boundary layer formulation and an envelope e^n transition criterion. The entire viscous solution (boundary layers and wake) is strongly interacted with the incompressible potential flow via the surface transpiration model. This permits proper calculation of limited separation regions. The drag is determined from the wake
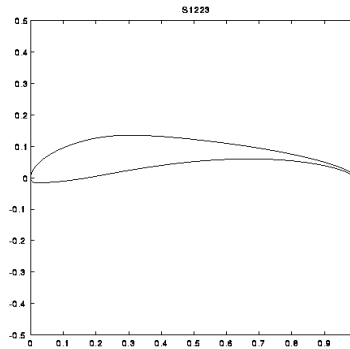

Figure 1. Selig 1223 airfoil geometry

momentum thickness far downstream. A special treatment is used for a blunt trailing edge which fairly accurately accounts for base drag. The total velocity at each point on the airfoil surface and wake, with contributions from the freestream, the airfoil surface vorticity, and the equivalent viscous source distribution, is obtained from the panel solution with the Karman-Tsien compressibility correction added, when necessary. This is incorporated into the viscous equations, yielding a nonlinear elliptic system which is readily solved by a full-Newton method.

2.2. Mathematical Model and Numerical Method

The airfoil contour and wake trajectory are discretized into flat panels, with N panel nodes on the airfoil, and N_w nodes on the wake. A linear vorticity distribution is associated with each airfoil panel. Each airfoil and wake panel also has a constant source strength related to viscous layer quantities. The stream function is given by:

$$\psi(x,y) = u_\infty y - v_\infty x + \frac{1}{2\pi}\int \gamma(s)\ln r(s;x,y)ds + \frac{1}{2\pi}\int \sigma(s)\vartheta(s;x,y)ds \qquad (1)$$

where s is the coordinate along the airfoil surface, r is the magnitude of the vector from the surface point at s and the field point (x,y), ϑ is the angle of the vector, and u_∞ and v_∞ are the x and y components of the undisturbed freestream velocity.

The viscous formulation is based on the ISES code written by Drela and Giles (1987). The streamline along the boundary layer edge, where the velocity is u_e, is displaced normal to the wall by a distance equal to the local displacement thickness δ^*. The present formulation employs the following standard integral momentum and kinetic energy shape parameter equations based on the streamwise coordinate ξ:

$$\frac{C_f}{2} = \frac{d\theta^*}{d\xi} + (2 + H - M_e^2)\frac{\theta^*}{u_e}\frac{du_e}{d\xi} \tag{2}$$

$$\theta^* \frac{dH^*}{d\xi} + [2H^{**} + H^*(1-H)]\frac{\theta^* du_e}{u_e d\xi} = 2C_D - H^*\frac{C_f}{2} \tag{3}$$

Here $H = \delta^*/\theta$ is the shape parameter, $H^* = \theta^*/\theta$ is the kinetic energy shape parameter and θ is the momentum layer thickness. Also a kinetic energy layer thickness θ^* is defined along with a maximum shear layer coefficient C_τ that represents a measure of the shear stresses in the wake. A shear stress lag equation, which has been slightly modified from the original formulation to improve the lift and drag prediction near stall, is used in turbulent flow regions.

$$\frac{\delta}{C_\tau}\frac{dC_\tau}{d\xi} = 5.6\left(C_{\tau_{EQ}}^{1/2} - C_\tau^{1/2}\right) + 2\delta\left\{\frac{4}{3\delta^*}\left[\frac{C_f}{2} - \left(\frac{H_k - 1}{6.7H_k}\right)^2\right] - \frac{1}{u_e}\frac{du_e}{d\xi}\right\} \tag{4}$$

For the laminar regions, Eq. (36) is replaced by a rate equation that models the growth of the amplitude n of the most amplified Tollmien-Schlichting wave.

$$\frac{dn}{d\xi} = \frac{dn}{d\,\mathrm{Re}_\theta} H_k \frac{d\,\mathrm{Re}_\theta}{d\xi}\left(H_k, \theta^*\right) \tag{5}$$

The Reynolds number Re_θ is based on the momentum layer thickness. The empirical relation dn/Re_θ is a correlation of spatial growth rates computed from solutions to the Orr-Sommerfeld equation and $Re_\theta/d\xi$ is obtained from the properties of the Falkner-Skan profile family. The transition point is defined by the location where n reaches a user-specified critical value n_{crit}. This parameter is in practice used to represent the background disturbance level and has a dramatic effect on low Reynolds number airfoil performance. The governing equations, Eqs. (2) to (5), are discretized using two-point central differences. The boundary layer variables θ, δ^* and C_τ or n and u_e are defined to be located at the panel nodes. In laminar regions, n replaces C_τ. Each panel therefore has three coupled nonlinear equations associated with it. The influence of the viscous layer on the potential flow is modeled by the wall transpiration concept if the local source strength σ is equal to the local gradient of mass defect, $\lambda \equiv u_e\delta$.

$$\sigma_i = \frac{d\lambda}{d\xi} = \pm\frac{\lambda_{i+1} - \lambda_i}{s_{i+1} - s_i} \tag{6}$$

This source distribution is then used to calculate u_e in the wake.

$$u_{e_i} = \nabla\psi.\hat{n} = u_\infty\hat{n}_x - v_\infty\hat{n}_y + \sum_{j=1}^{N} c_{ij}^\gamma \gamma_j \sum_{j=1}^{N+N_W-1} c_{ij}^\sigma \sigma_j \tag{7}$$

Equation (7) is used to solve for the three unknown variables θ, δ^* and C_τ, in the three Eqs. (2), (3), (4) and (5). The resulting value of δ^* gives a new source distribution, Eq. (6), for the inviscid calculation where the new boundary layer edge velocity distribution is obtained.

3. NUMERICAL ANALYSIS USING FLUENT

3.1. Introduction to Fluent

Fluent is a CFD software based on the solution of the Navier-Stokes equations using the finite-volume method. It is widely used in the aerospace, automobilist, chemical and micro-electronic industries.

3.2. Governing Equations

Fluent solves conservation equations for mass and momentum. The general form of the continuity equation is given by,

$$\frac{\partial \rho}{\partial t} + \frac{\partial}{\partial x_i}(\rho u_i) = S_m \tag{8}$$

where S_m is a source term. Conservation of momentum in the i direction in a inertial reference frame is given,

$$\frac{\partial}{\partial t}(\rho u_i) + \frac{\partial}{\partial x_j}(\rho u_i u_j) = -\frac{\partial p}{\partial x_i} + \frac{\partial \tau_{ij}}{\partial x_j} + \rho g_i + F_i \tag{9}$$

where p is the static pressure, τ_{ij} is the stress tensor, ρg_i and F_i are respectively the gravitational body force and the external body forces in the i direction. The stress tensor τ_{ij} is given by

$$\tau_{ij} = \left[\mu \left(\frac{\partial u_i}{\partial x_j} + \frac{\partial u_j}{\partial x_i} \right) \right] - \frac{2}{3} \mu \frac{\partial u_i}{\partial x_i} \delta_{ij} \tag{10}$$

3.3. The Spalart-Allmaras One-Equation Turbulence Model

This turbulence model was proposed by Spalart and Allmaras (1992) and it solves a transport equation for a quantity that is a modified form of the turbulent kinematic viscosity. The transported variable, $\overline{v}$, is identical to the turbulent kinematic viscosity except in the viscous affected region. The transport equation for $\overline{v}$ is

$$\rho \frac{D\overline{v}}{Dt} = G_v + \frac{1}{\sigma_{\overline{v}}} \left\{ \frac{\partial}{\partial x_j} \left[(\mu + \rho \overline{v}) \frac{\partial \overline{v}}{\partial x_j} \right] + C_{b2} \rho \left(\frac{\partial \overline{v}}{\partial x_j} \right)^2 \right\} - Y_v \tag{11}$$

where G_v and Y_v are, respectively, the production and destruction of turbulent viscosity that occurs in the near-wall region, $\sigma_{\overline{v}}$ and C_{b2} are constants and v is the molecular kinematic viscosity.

The modified turbulent kinematic viscosity, $\overline{v}$, is set to zero at walls. When the mesh is sufficiently fine, so that it can resolve the laminar sublayer, the wall shear stress is obtained from the laminar stress-strain relationship:

$$\frac{u}{u_\tau} = \frac{\rho u_\tau y}{\mu} \tag{12}$$

Fluent has implemented the boundary conditions for the S-A model so that it can work on coarse meshes using wall functions, instead. When it is the case, it is assumed that the centroid of the wall-adjacent cell falls within the logarithmic region of the boundary layer, and the law of the wall is employed:

$$\frac{u}{u_\tau} = \frac{1}{\kappa} \ln E\left(\frac{\rho u_\tau y}{\mu}\right) \tag{13}$$

where κ=0.419 and E=9.793.

3.4. The Realizable k-ε Two-Equation Turbulence Model

The Realizable k-ε model is a variant of the standard k-ε and it was proposed by Shih, Liou and Zhu (1995). It was intended to overcome some deficiencies of the traditional k-ε models by adopting a new eddy-viscosity formula involving a variable C_μ originally proposed by Reynolds (1987) and a new model equation for dissipation, ε, based on the dynamic equation of the mean-square vorticity fluctuation. The modeled transport equations for k and ε are:

$$\rho \frac{Dk}{Dt} = \frac{\partial}{\partial x_j}\left[\left(\mu + \frac{\mu_t}{\sigma_k}\right)\frac{\partial k}{\partial x_j}\right] + G_k + G_b - \rho\varepsilon - Y_M \tag{14}$$

and

$$\rho \frac{D\varepsilon}{Dt} = \frac{\partial}{\partial x_j}\left[\left(\mu + \frac{\mu_t}{\sigma_\varepsilon}\right)\frac{\partial \varepsilon}{\partial x_j}\right] + \rho C_1 S\varepsilon - \rho C_2 \frac{\varepsilon^2}{k + \sqrt{\nu\varepsilon}} + C_{1\varepsilon}\frac{\varepsilon}{k}C_{3\varepsilon}G_b \tag{15}$$

where

$$C_1 = \max\left[0.43, \frac{\eta}{\eta + 5}\right] \tag{16}$$

and

$$\eta = \frac{Sk}{\varepsilon} \tag{17}$$

G_k and G_b represent the generation of turbulent kinetic energy due to mean velocity gradients and buoyancy, respectively. Y_M is the contribution of the fluctuating dilatation in the compressible turbulence to the overall dissipation rate. C_2 and $C_{1\varepsilon}$ are constants. σ_k and σ_e are the turbulent Prandtl numbers for k and ε, respectively. The eddy viscosity is calculated from Eq. (18) with C_μ no longer being constant. It now is a function of the mean strain and rotation rates, the angular velocity of the system rotation and the turbulence fields.

$$\mu_t = \rho C_\mu \frac{k^2}{\varepsilon} \tag{18}$$

3.5. Near-Wall Treatment

In the numerical simulations of the present work it will be used the low-Reynolds numbers approximation for the near-wall region. For the Spalart-Allmaras turbulence model, the mesh should be sufficiently fine so that the low-Reynolds numbers approximation can be automatically set by Fluent. For the Realizable k-ε turbulence model, the Fluent version of the low-Reynolds numbers approximation, called "Two-Layer Zonal", is selected and then the mesh should be fine in the near-wall region. The y^+ (non-dimensional node distance to the wall) values should be equal to or less than the unity.

The whole domain is subdivided into a viscosity-affected region and a fully-turbulent region. The demarcation of the two regions is determined by a wall-distance based turbulent Reynolds number, Re_y, given by

$$\mathrm{Re}_y = \frac{\rho \sqrt{k}\, y}{\mu} \qquad (19)$$

The fully-turbulent region is defined by $Re_y > 200$, and there the k-ε model is employed. In equation (19) y is the normal distance from the cell center to the wall. The viscosity-affected region is defined by $Re_y < 200$, and there the one-equation model of Wolfstein (1969) is employed. For this region, the turbulent viscosity and the ε field are given, respectively, by:

$$\mu_t = \rho C_\mu \sqrt{k}\, \ell_\mu \qquad (20)$$

$$\varepsilon = \frac{k^{3/2}}{\ell_\varepsilon} \qquad (21)$$

The length scales ℓ_μ and ℓ_ε are computed from:

$$\ell_\mu = c_\ell y \left[1 - \exp\left(-\frac{\mathrm{Re}_y}{A_\mu} \right) \right] \qquad (22)$$

$$\ell_\varepsilon = c_\ell y \left[1 - \exp\left(-\frac{\mathrm{Re}_y}{A_\varepsilon} \right) \right] \qquad (23)$$

The constants of Eqs. (22) and (23) were taken from Chen and Patel (1988). They are $c_\ell = \kappa C_\mu^{-3/4}$, $A_\mu = 70$ and $A_\varepsilon = 2c_\ell$.

3.6. Grid Generation

It was used a structured C-type grid that was generated using Gambit. The external boundaries of the grid are on the order of more than 10 times the airfoil chord. First, a study of grid independence was made. The results for lift and drag coefficients, C_L and C_D, respectively, are shown in Tab. (1). The results were taken until convergence was achieved ($1x10^{-6}$ for the continuity equation residuals).

Table 1. Study of the grid independence

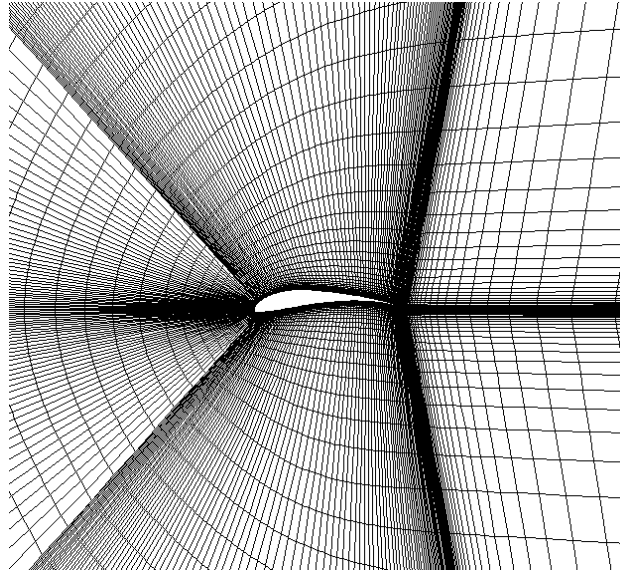| Total number of cells	Cells near the airfoil surface in the normal direction	C_L	C_D
10200	20	1.137	0.0287
14200	30	1.138	0.0274
18360	40	1.142	0.0270
21760	50	1.142	0.0270

Figure 2. A detail of the grid

Special attention was given to the regions where large pressure or velocity gradients were expected, like the normal direction to the airfoil surface and the downstream direction near the airfoil leading edge. A detail of the final grid is shown in Fig. (2).
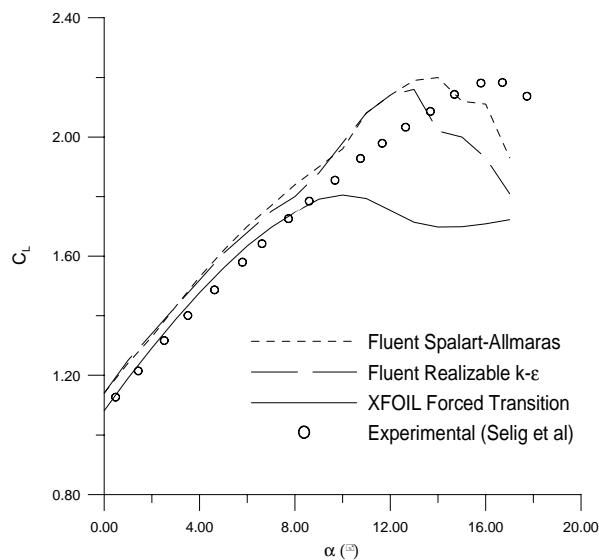
Figure 3. Lift curve

3.7. Boundary Conditions

To achieve the desired chord-based Reynolds number of the experimental results (2×10^5), the inlet velocity is set equal to the freestream velocity of 11.69 m/s. Wall boundary conditions are

applied to the airfoil top and bottom surfaces. The fluid contained in the interior region is air (ρ = 1.225 kg/m^3 and μ = 1.79x10^{-5}).

To simulate the airfoil with angle of attack, the freestream velocity vector was decomposed into two orthogonal components not aligned with the original Fluent system of coordinates. It gives the advantage to simulate all angles of attack with one grid only, but the results output by Fluent are still based on its original system of coordinates and a transformation of coordinates is needed, as given by Eqs. (24) and (25).
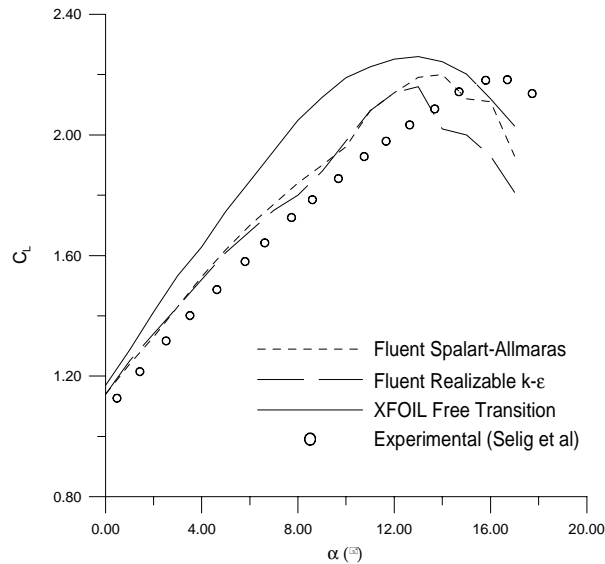

Figure 4. Lift curve

$$L = L'\cos(\alpha) - D'\text{sen}(\alpha) \tag{24}$$

$$D = L'\text{sen}(\alpha) + D'\cos(\alpha) \tag{25}$$

where L and D are lift and drag, respectively, L' and D' are components of aerodynamic force based on the original system of coordinates of Fluent and α is the angle of attack.

4.RESULTS

Figures (3) and (4) show the results obtained for the lift coefficient. For both FLUENT turbulence models the agreement is good until the incidence of approximately 9º. It can be noted the difference between the results calculated by XFOIL with free and forced transition. When the transition is fixed in the leading edge, the agreement with the experimental results is good until the incidence of 8º, but the maximum lift coefficient is under predicted. With the free transition point calculated, the maximum lift coefficient is well predicted, although it occurs in a lower angle of attack.

The polar drag plots for this airfoil are shown in Figs. (5) and (6). Both turbulence models of Fluent overpredict the drag coefficient values. It is interesting to note that the XFOIL results agree much better with the experimental ones when the transition point is calculated, as expected.

The viscous and pressure drag for 0º incidence are presented separately in Tab. (2). It is clear that the FLUENT code overestimates the pressure drag. It also can be noted the difference in the viscous drag when the transition point is not calculated.

Table 2. Viscous and pressure drag for the different models at 0º incidence

Pressure drag coefficient (C_{Dp})				Viscous drag coefficient (C_{Df})			
Spal-Allm	Real k-ε	XFOIL forced trans	XFOIL free transition	Spal-Allm	Real k-ε	XFOIL forced trans	XFOIL free transition
0.015	0.018	0.009	0.009	0.012	0.014	0.012	0.008

Figures (7) and (8) finally show the pressure coefficient distribution through the chord for the angles of attack 0º and 5º, respectively.

The agreement between the computed results for the different models is good until x/c equals approximately 0.6. This means that the pressure gradients were different downstream this point, the same will happen to the prediction of the separation point and consequently the drag coefficients computed will also be different.
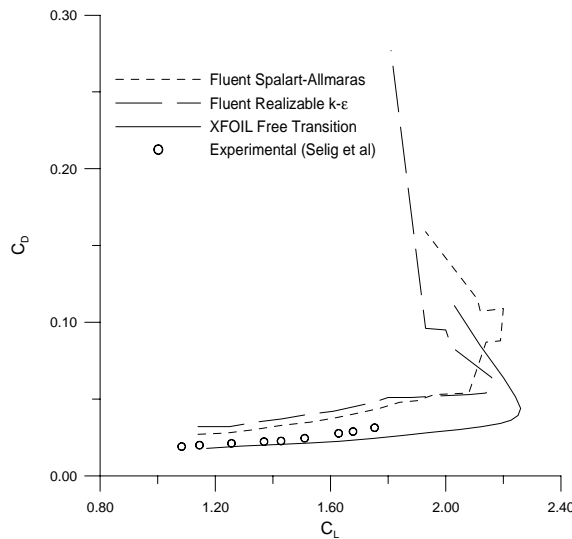

Figure 5. Polar drag

5. CONCLUSIONS

Two different turbulence models were used in Fluent calculations and XFOIL calculations were performed using forced transition at the leading edge and letting the code calculate the transition point (free transition).

The computed lift coefficients have good agreement to the experimental values up to approximately 8º. The prediction of the maximum lift coefficient value is good, except for the XFOIL with forced transition case, although the incidence it occurs cannot be correctly predicted.

The drag coefficient values computed by Fluent are always overpredicted. A significant difference between the values of drag coefficients (and the maximum lift coefficient) is found when employing or not the calculation of the transition point. It emphasizes the importance of calculating the onset of transition.

6. REFERENCES

Cebeci, T., Besnard, E. and Chen, H.H., 1998, "An interactive Boundary-Layer Method for Multielement Airfoils", Computer & Fluids, Vol. 27, No. 5-6, pp.651-661.

Chen, H.C. and Patel, V.C., 1988, "Near-Wall Turbulence Models for Complex Flows Including Separation", AIAA Journal, 26(6), pp. 641-648.

Drela, M. and Giles, M.B., 1987, "ISES: A Two-Dimensional Viscous Aerodynamic Design and Analysis Code", AIAA-87-0424, American Institute of Aeronautics and Astronautics.

Drela, M. and Giles, M.B., 1987, "Viscous-Inviscid Analysis of Transonic and Low-Reynolds Number Airfoils", AIAA Journal, Vol. 25(10), pp.1347-1355.

Reynolds, W.C., "Fundamentals of turbulence for turbulence modeling and simulation", Lecture Notes for Von Karman Institute Agard Report No. 755.

Schlichting, H., 1979, "Boundary-Layer Theory", Mc-Graw Hill, New York, USA, 817 pp.

Selig, M.S., Guglielmo, J.J., Broeren, A.P. and Giguere, P., 1996, "Summary of Low-Speed Airfoil Data", SoarTech Publications, Vol. 2, May 1996.

Shih, T.-H., Liou, W.W., Shabbir, A. and Zhu, J., 1995, "A New k-e Eddy-Viscosity Model for High Reynolds Number Turbulent Flows - Model Development and Validation", Computers Fluids, 24(3), pp. 227-238.

Spalart, P. and Allmaras, S., 1992, "A one-equation turbulence model for aerodynamic flows", Technical Report AIAA-92-0439, American Institute of Aeronautics and Astronautics.

Wolfstein, M., 1969, "The Velocity and Temperature Distribution of One-Dimensional Flow with Turbulence Augmentation and Pressure Gradient", Int. J. Heat Mass Transfer, 12, pp. 301-318.
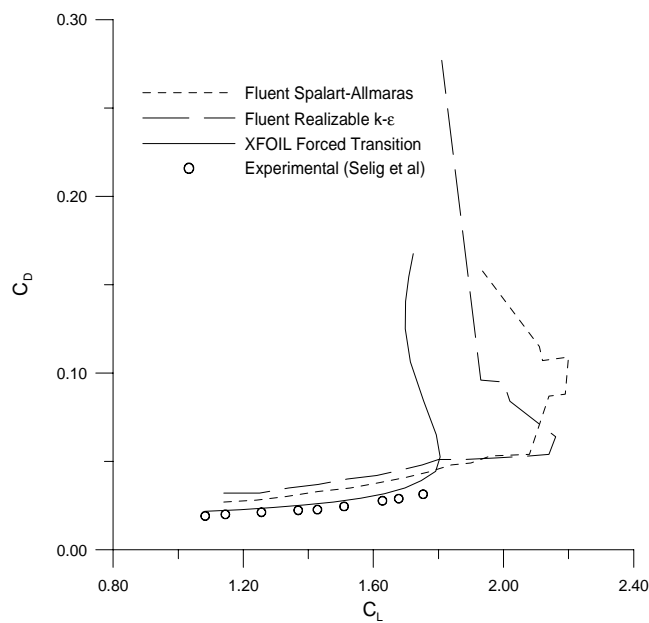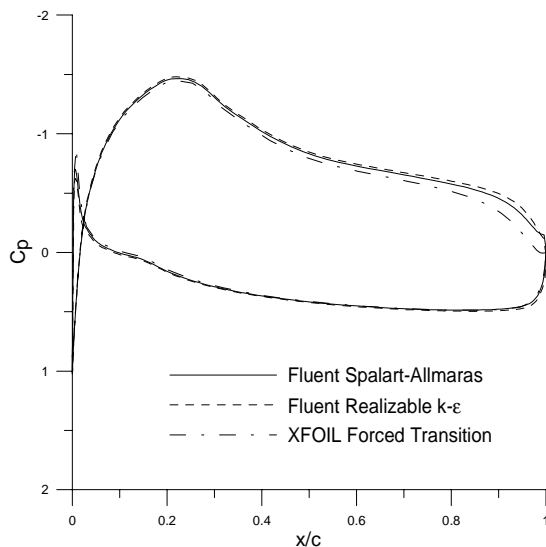
Figure 6. Polar Drag

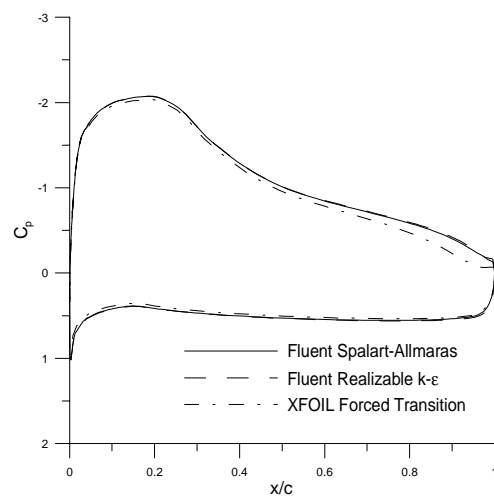Figure 7. C_p distribution (0° incidence)

Figure 8. C_p distribution (0° incidence)